PERGAMON

International Journal of Solids and Structures 40 (2003) 881–897

INTERNATIONAL JOURNAL OF SOLIDS and STRUCTURES

www.elsevier.com/locate/ijsolstr

A circular inclusion with a nonuniform interphase layer in anti-plane shear

X. Wang *, Z. Zhong

Key Laboratory of Solid Mechanics of MOE, Department of Engineering Mechanics and Technology, Tongji University, Shanghai 200092, PR China

Received 29 December 2001; received in revised form 5 November 2002

Abstract

An analytical solution is derived for the problem of a nonuniformly coated circular inclusion in an unbounded matrix under anti-plane deformations. The inclusion/interphase/matrix system is subject to (1) remote uniform shear and uniform eigenstrain imposed on the circular inclusion, and (2) a screw dislocation or a point force in the matrix. It is found that the varying interphase thickness will exert a significant influence on the nonuniform stress field within the circular inclusion, and on the direction and magnitude of the image force acting on a screw dislocation. In the course of development, it is found that the presence of certain coated inclusions, which are termed *stealth*, will not cause change of elastic energy in the body. The derived analytical solution for a screw dislocation is then employed as Green's function to investigate a radial matrix crack interacting with the nonuniformly coated inclusion. The numerical results show that the varying interphase thickness will also affect the stress intensity factors.

Keywords: Circular inclusion; Interphase; Screw dislocation; Anti-plane shear

1. Introduction

The interphases between the fiber and the surrounding matrix have become a focused research topic in recent years due to the fact that the interphases, although usually small in thickness, can affect the overall mechanical properties of the fiber-reinforced composites, and play an important role in controlling the failure mechanism and fracture toughness of composite materials. Up to now, two different kinds of models have been proposed and developed to simulate the interphase layer. One widely used model (see, for example Achenbach and Zhu, 1990; Zhong and Meguid, 1997; Ru and Schiavone, 1997; Shen et al., 2000, 2001a,b; Liu et al., 2001) is based on the assumption that tractions are continuous but displacements are discontinuous across the interface. More precisely, jumps in the displacement components are assumed to be proportional, in terms of the 'spring-factor-type' interface parameters, to their respective interface

* Corresponding author.
E-mail address: wjq_wang@sina.com (X. Wang).

0020-7683/02/$ - see front matter
PII: S0020-7683(02)00644-3

traction components. As pointed out by Liu et al. (2000), the main drawbacks of this spring-like model lie in that it cannot provide other important information about the property of the composite, such as the effect of changes of thickness and nonuniform distribution of the interphases. The other model (see, for example Honein et al., 1994; Ru et al., 1999; Liu et al., 2000; Xiao and Chen, 2000, 2001a,b; Shodja and Sarvestani, 2001), which is based on strict elasticity theory and which will be employed in this study, assumes the interphase as a distinct layer between the fiber (inclusion) and the matrix, of specified thickness and of elastic constants different from those of the matrix and the fiber.

The main objectives of the present paper are (1) to investigate the influence of varying interphase thickness on the stress fields induced within and near the fiber (inclusion); (2) to probe the influence of varying interphase thickness on the mobility of a dislocation in the matrix; and (3) to study the influence of varying interphase thickness on matrix cracking. By applying complex variable techniques, an exact elastic solution in series form is derived for the interaction problem between a nonuniformly coated inclusion and a screw dislocation or a point force. The derived analytical solution for a screw dislocation is then utilized as Green's function to investigate matrix cracking in the inclusion/interphase/matrix system. The numerical results show clearly how the nonuniform stress field, average stresses and peak stresses within the circular inclusion, change of elastic energy due to the introduction of the coated inclusion, and stress concentration vary with the nonuniformity of the interphase thickness when the composite system is only subject to remote uniform shearing and uniform eigenstrain imposed on the circular inclusion. The numerical results also convincingly demonstrate that varying interphase thickness can significantly affect the direction and magnitude of the image force acting on a screw dislocation in the matrix, and can influence the stress intensity factors (SIF) for a matrix crack.

2. Basic equations

As shown in Fig. 1, we consider a circular inclusion S_3 surrounded by an interphase layer S_2 of nonuniform thickness, which in turn is embedded in an unbounded matrix S_1. The shear moduli of S_1, S_2 and S_3 are respectively μ_1, μ_2 and μ_3. Both the outer circular interface Γ_1 formed by S_1 and S_2, and the inner circular interface Γ_2 formed by S_3 and S_2 are assumed to be perfect, i.e., both tractions and displacements are continuous across the two interfaces. The origin of the Cartesian coordinate system is chosen to be at the center of the outer circle Γ_1 of unit radius. The center of the inner circle Γ_2 of radius $R_0 = (x_2 - x_1)/2$

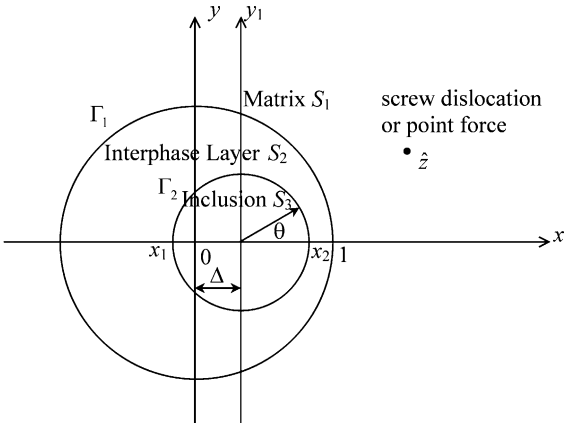

Fig. 1. A screw dislocation or a point force near a circular inclusion with a nonuniform interphase layer (z-plane).

lies on the x-axis. The two centers of the two circles Γ_1 and Γ_2 are set apart by the distance $\Delta = (x_1 + x_2)/2$. The composite system is subject to remote uniform anti-plane shearing $\{\sigma_{zx}^{\infty}, \sigma_{zy}^{\infty}\}$ and uniform anti-plane eigenstrains $\{\varepsilon_{zx}^{*}, \varepsilon_{zy}^{*}\}$ imposed on the circular inclusion S_3. In addition, a line force $\hat{f}$ or a screw dislocation with Burgers vector $\hat{b}$ is located at the point $\hat{z} = \hat{x} + \mathrm{i}\hat{y}$ in the matrix. The nonvanishing stress components are σ_{zx} and σ_{zy} and the only displacement component is the out-of-plane component u_z. For this anti-plane deformation state, the out-of-plane displacement u_z and stress components can be expressed in terms of a complex function $f(z)$ ($z = x + \mathrm{i}y$) as follows (Muskhelishvili, 1953; Gong and Meguid, 1992)

$$\begin{aligned} u_z &= \mathrm{Im}\{f(z)\} \\ \sigma_{zy} + \mathrm{i}\sigma_{zx} &= \mu f'(z) \end{aligned} \tag{1}$$

The complex potentials defined in the regions S_1, S_2 and S_3 will be denoted by $f_1(z)$, $f_2(z)$ and $f_3(z)$.

3. Conformal mapping

We adopt the following conformal mapping function $m(\zeta)$ (Cao, 1988)

$$z = m(\zeta) = \frac{\zeta - a}{a\zeta - 1} \tag{2}$$

where

$$a = \frac{1 + x_1 x_2 + \sqrt{(x_1^2 - 1)(x_2^2 - 1)}}{x_1 + x_2} > 1 \tag{3}$$

The mapped ζ-plane is shown in Fig. 2. It can be observed that the unbounded matrix S_1 is mapped onto a unit disk $|\zeta| < 1$ in the ζ-plane and the point at infinity $z = \infty$ is mapped onto $\zeta = 1/a$ in the ζ-plane, the interphase layer S_2 formed by two eccentric circles Γ_1 and Γ_2 is mapped onto the annulus $1 < |\zeta| < R$ ($R = (1 - x_1 x_2 + \sqrt{(x_1^2 - 1)(x_2^2 - 1)})/(x_2 - x_1) > 1$) in the ζ-plane, and the circular inclusion S_3 is mapped onto $|\zeta| > R$ in the ζ-plane. It's easier to solve the boundary value problem in the ζ-plane than in the original z-plane.

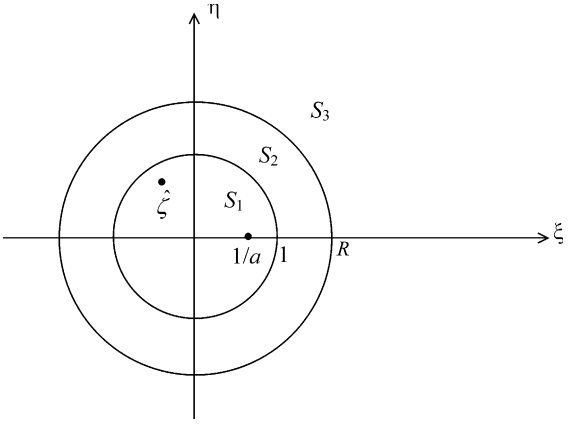

Fig. 2. The problem in the ζ-plane.

4. Exact solution

4.1. Field potentials

It shall be mentioned here that for convenience, we write

$$f_i(z) = f_i(m(\zeta)) = f_i(\zeta) \quad (i = 1, 2, 3)$$

The continuity condition of displacement across the interface $|\sigma| = 1$ can be expressed as

$$[f_1(\sigma) + \overline{f}_2(1/\sigma)]^+ = [\overline{f}_1(1/\sigma) + f_2(\sigma)]^- \quad (|\sigma| = 1) \tag{4}$$

where the superscripts "+" and "−" denote the limit values from the inner and outer sides of the contour being considered.

In view of the above expression, we introduce a function $\Delta_1(\zeta)$ defined by

$$\Delta_1(\zeta) = \begin{cases} f_1(\zeta) + \overline{f}_2(1/\zeta) & 1/R < |\zeta| < 1 \\ \overline{f}_1(1/\zeta) + f_2(\zeta) & 1 < |\zeta| < R \end{cases} \tag{5}$$

By the generalized Liouville's theorem, we can obtain

$$\Delta_1(\zeta) = \frac{K}{\zeta - 1/a} - \frac{a^2\overline{K}}{\zeta - a} + q \ln\frac{\zeta - \hat{\zeta}}{\zeta - 1/a} + \bar{q} \ln\frac{\zeta - 1/\bar{\hat{\zeta}}}{\zeta - a} + \sum_{n=1}^{+\infty}(A_n\zeta^n + \overline{A}_n\zeta^{-n}) \quad (1/R < |\zeta| < R) \tag{6}$$

where

$$K = \frac{a^{-2} - 1}{\mu_1}(\sigma_{zy}^{\infty} + \mathrm{i}\sigma_{zx}^{\infty}), \quad q = \frac{\hat{b} - \mathrm{i}\mu_1^{-1}\hat{f}}{2\pi}, \quad \hat{\zeta} = \frac{\hat{z} - a}{a\hat{z} - 1} \tag{7}$$

The continuity condition of traction across the interface $|\sigma| = 1$ can be expressed as

$$\mu_1[f_1^+(\sigma) + \overline{f}_1^-(1/\sigma)] = \mu_2[f_2^-(\sigma) + \overline{f}_2^+(1/\sigma)] \quad (|\sigma| = 1) \tag{8}$$

Inserting Eq. (6) into Eq. (8) and eliminating $f_2^-(\sigma)$, $\overline{f}_2^+(1/\sigma)$ will yield

$$f_1^+(\sigma) + \overline{f}_1^-(1/\sigma) = \eta_1\Delta_1(\sigma) \quad (|\sigma| = 1) \tag{9}$$

where

$$\eta_1 = \frac{2\mu_2}{\mu_1 + \mu_2} \tag{10}$$

In view of Eq. (9), we introduce an auxiliary function $\Omega_1(\zeta)$ defined by

$$\Omega_1(\zeta) = \begin{cases} f_1(\zeta) + (1 - \eta_1)\left[-\dfrac{a^2\overline{K}}{\zeta - a} + \bar{q}\ln\dfrac{\zeta - 1/\bar{\hat{\zeta}}}{\zeta - a}\right] - \eta_1\sum\limits_{n=1}^{+\infty}A_n\zeta^n - q\ln\dfrac{\zeta - \hat{\zeta}}{\zeta - 1/a} - \dfrac{K}{\zeta - 1/a} & (|\zeta| < 1) \\ -\overline{f}_1(1/\zeta) - (1 - \eta_1)\left[\dfrac{K}{\zeta - 1/a} + q\ln\dfrac{\zeta - \hat{\zeta}}{\zeta - 1/a}\right] + \eta_1\sum\limits_{n=1}^{+\infty}\overline{A}_n\zeta^{-n} + \bar{q}\ln\dfrac{\zeta - 1/\bar{\hat{\zeta}}}{\zeta - a} - \dfrac{a^2\overline{K}}{\zeta - a} & (|\zeta| > 1) \end{cases} \tag{11}$$

It follows from Eqs. (9) and (11) that $\Omega_1(\zeta)$ is analytic and single-valued in the whole complex ζ-plane including the point at infinity. By Liouville's theorem, we obtain

$$\Omega_1(\zeta) \equiv 0 \tag{12}$$

then

$$\begin{aligned} f_1(\zeta) &= (1-\eta_1)\left[\frac{a^2\overline{K}}{\zeta-a} - \bar{q}\ln\frac{\zeta-1/\bar{\hat{\zeta}}}{\zeta-a}\right] + \eta_1\sum_{n=1}^{+\infty}A_n\zeta^n + q\ln\frac{\zeta-\hat{\zeta}}{\zeta-1/a} + \frac{K}{\zeta-1/a} \quad (|\zeta|<1) \\ \overline{f}_1(1/\zeta) &= (1-\eta_1)\left[-\frac{K}{\zeta-1/a} - q\ln\frac{\zeta-\hat{\zeta}}{\zeta-1/a}\right] + \eta_1\sum_{n=1}^{+\infty}\overline{A}_n\zeta^{-n} + \bar{q}\ln\frac{\zeta-1/\bar{\hat{\zeta}}}{\zeta-a} - \frac{a^2\overline{K}}{\zeta-a} \quad (|\zeta|>1) \end{aligned} \tag{13}$$

Substituting Eq. $(13)_2$ into Eq. (5) will lead to the following expression for $f_2(\zeta)$

$$f_2(\zeta) = (2-\eta_1)\left[\frac{K}{\zeta-1/a} + q\ln\frac{\zeta-\hat{\zeta}}{\zeta-1/a}\right] + \sum_{n=1}^{+\infty}\left[A_n\zeta^n + (1-\eta_1)\overline{A}_n\zeta^{-n}\right] \quad (1<|\zeta|<R) \tag{14}$$

The continuity condition of displacement across the interface $|\tau| = R$ can be expressed as

$$\left[f_2(\tau) + \overline{f}_3(R^2/\tau) - \frac{2(aR)^2\overline{\omega}}{\tau-aR^2}\right]^+ = \left[\overline{f}_2(R^2/\tau) + f_3(\tau) + \frac{2\omega}{\tau-1/a}\right]^- \quad (|\tau|=R) \tag{15}$$

where

$$\omega = (a^{-2}-1)(\varepsilon^*_{zy} + \mathrm{i}\varepsilon^*_{zx}) \tag{16}$$

In view of the above expression, we introduce a function $\Delta_2(\zeta)$ defined by

$$\Delta_2(\zeta) = \begin{cases} f_2(\zeta) + \overline{f}_3(R^2/\zeta) - \dfrac{2(aR)^2\overline{\omega}}{\zeta-aR^2} & (1<|\zeta|<R) \\ \overline{f}_2(R^2/\zeta) + f_3(\zeta) + \dfrac{2\omega}{\zeta-1/a} & (R<|\zeta|<R^2) \end{cases} \tag{17}$$

By the generalized Liouville's theorem, we can obtain

$$\Delta_2(\zeta) = \sum_{n=1}^{+\infty}(B_n\zeta^n + \overline{B}_nR^{2n}\zeta^{-n}) \quad (1<|\zeta|<R^2) \tag{18}$$

The continuity condition of traction across the interface $|\tau| = R$ can be expressed as

$$\mu_2[f_2^+(\tau) + \overline{f}_2^-(R^2/\tau)] = \mu_3[f_3^-(\tau) + \overline{f}_3^+(R^2/\tau)] \quad (|\tau|=R) \tag{19}$$

Inserting Eq. (17) into Eq. (19) and eliminating $f_2^+(\tau)$, $\overline{f}_2^-(R^2/\tau)$ will yield

$$f_3^+(\tau) + \overline{f}_3^-(R^2/\tau) = \eta_2\left[\Delta_2(\tau) + \frac{(aR)^2\overline{\omega}}{\tau-aR^2} - \frac{\omega}{\tau-1/a}\right] \quad (|\tau|=R) \tag{20}$$

where

$$\eta_2 = \frac{2\mu_2}{\mu_2+\mu_3} \tag{21}$$

In view of Eq. (20), we introduce a function $\Omega_2(\zeta)$ defined by

$$\Omega_2(\zeta) = \begin{cases} f_3(\zeta) - \eta_2\left[\displaystyle\sum_{n=1}^{+\infty}\overline{B}_nR^{2n}\zeta^{-n} - \frac{\omega}{\zeta-1/a}\right] & (|\zeta|>R) \\ -\overline{f}_3(R^2/\zeta) + \eta_2\left[\displaystyle\sum_{n=1}^{+\infty}B_n\zeta^n + \frac{(aR)^2\overline{\omega}}{\zeta-aR^2}\right] & (|\zeta|<R) \end{cases} \tag{22}$$

It can be easily deduced from Eqs. (20) and (22) that

$$\Omega_2(\zeta) \equiv 0 \tag{23}$$

then

$$\begin{aligned} f_3(\zeta) &= \eta_2 \left[\sum_{n=1}^{+\infty} \overline{B}_n R^{2n} \zeta^{-n} - \frac{\omega}{\zeta - 1/a} \right] \quad (|\zeta| > R) \\ \overline{f}_3(R^2/\zeta) &= \eta_2 \left[\sum_{n=1}^{+\infty} B_n \zeta^n + \frac{(aR)^2 \overline{\omega}}{\zeta - aR^2} \right] \quad (|\zeta| < R) \end{aligned} \tag{24}$$

Substituting Eq. $(24)_2$ into Eq. (17) will yield

$$f_2(\zeta) = \sum_{n=1}^{+\infty} \left[(1-\eta_2) B_n \zeta^n + \overline{B}_n R^{2n} \zeta^{-n} + (2-\eta_2) \frac{(aR)^2 \overline{\omega}}{\zeta - aR^2} \right] \quad (1 < |\zeta| < R) \tag{25}$$

In order to simultaneously satisfy the boundary conditions at Γ_1 and Γ_2, the compatibility condition for $f_2(\zeta)$ shall be satisfied. The compatibility condition for $f_2(\zeta)$ will lead to the following two compatibility identities

$$\begin{aligned} &\sum_{n=1}^{+\infty} \left[(1-\eta_1) \overline{A}_n - \overline{B}_n R^{2n} \right] \zeta^{-n} = (\eta_1 - 2) \left[\frac{K}{\zeta - 1/a} + q \ln \frac{\zeta - \hat{\zeta}}{\zeta - 1/a} \right] \\ &\sum_{n=1}^{+\infty} \left[A_n - (1-\eta_2) B_n \right] \zeta^n = (2-\eta_2) \frac{(aR)^2 \overline{\omega}}{\zeta - aR^2} \\ &\quad (1 < |\zeta| < R) \end{aligned} \tag{26}$$

Expanding all of the terms in the above expression and equating the coefficients of the same power of ζ will lead to the following set of algebraic equations

$$\begin{aligned} &(1-\eta_1) A_n - B_n R^{2n} = (\eta_1 - 2) \left[\overline{K} a^{1-n} - \bar{q} \left(\frac{\overline{\hat{\zeta}^n} - a^{-n}}{n} \right) \right] \\ &A_n = (1-\eta_2) B_n + (\eta_2 - 2) a (aR^2)^{-n} \overline{\omega} \\ &\quad \text{for } n = 1, 2, \ldots, +\infty \end{aligned} \tag{27}$$

Then all of the unknowns can be uniquely determined to be

$$\begin{cases} A_n = \dfrac{1}{(1-\eta_1)(1-\eta_2) - R^{2n}} \left\{ (1-\eta_2)(\eta_1 - 2) \left[\overline{K} a^{1-n} - \bar{q} \left(\dfrac{\overline{\hat{\zeta}^n} - a^{-n}}{n} \right) \right] + (2-\eta_2) a^{1-n} \overline{\omega} \right\} \\ B_n = \dfrac{1}{(1-\eta_1)(1-\eta_2) - R^{2n}} \left\{ (\eta_1 - 2) \left[\overline{K} a^{1-n} - \bar{q} \left(\dfrac{\overline{\hat{\zeta}^n} - a^{-n}}{n} \right) \right] + (2-\eta_2)(1-\eta_1) a^{1-n} R^{-2n} \overline{\omega} \right\} \\ \quad \text{for } n = 1, 2, \ldots, +\infty \end{cases} \tag{28}$$

Now, all of the holomorphic functions have been fully obtained as follows

$$\begin{aligned} f_1(\zeta) &= (1-\eta_1)\left[\frac{a^2\overline{K}}{\zeta-a} - \bar{q}\ln\frac{\zeta-1/\bar{\hat{\zeta}}}{\zeta-a}\right] + \eta_1\sum_{n=1}^{+\infty}A_n\zeta^n + q\ln\frac{\zeta-\hat{\zeta}}{\zeta-1/a} + \frac{K}{\zeta-1/a} \quad (|\zeta|<1) \\ f_2(\zeta) &= (2-\eta_1)\left[\frac{K}{\zeta-1/a} + q\ln\frac{\zeta-\hat{\zeta}}{\zeta-1/a}\right] + \sum_{n=1}^{+\infty}\left[A_n\zeta^n + (1-\eta_1)\overline{A}_n\zeta^{-n}\right] \\ &= \sum_{n=1}^{+\infty}\left[(1-\eta_2)B_n\zeta^n + \overline{B}_nR^{2n}\zeta^{-n} + (2-\eta_2)\frac{(aR)^2\overline{\omega}}{\zeta-aR^2}\right] \quad (1<|\zeta|<R) \\ f_3(\zeta) &= \eta_2\left[\sum_{n=1}^{+\infty}\overline{B}_nR^{2n}\zeta^{-n} - \frac{\omega}{\zeta-1/a}\right] \quad (|\zeta|>R) \end{aligned} \tag{29}$$

4.2. Stress field

- In the unbounded matrix S_1

$$\begin{aligned} \sigma_{zy}+\mathrm{i}\sigma_{zx} &= \sigma_{zy}^{\infty}+\mathrm{i}\sigma_{zx}^{\infty} + \frac{\mu_1 q(a\hat{\zeta}-1)(a\zeta-1)}{(\zeta-\hat{\zeta})} + \mu_1\frac{(a\zeta-1)^2}{a^2-1} \\ &\quad\times\left\{(\eta_1-1)\left[\frac{a^2\overline{K}}{(\zeta-a)^2} + \frac{\bar{q}(1-a\bar{\hat{\zeta}})}{(\bar{\hat{\zeta}}\zeta-1)(\zeta-a)}\right] + \eta_1\sum_{n=1}^{+\infty}nA_n\zeta^{n-1}\right\} \quad (|\zeta|<1) \end{aligned} \tag{30}$$

- In the intermediate interphase layer S_2

$$\begin{aligned} \sigma_{zy}+\mathrm{i}\sigma_{zx} &= \mu_2\frac{(a\zeta-1)^2}{a^2-1}\times\left\{(2-\eta_1)\left[-\frac{K}{(\zeta-1/a)^2} + \frac{q(a\hat{\zeta}-1)}{(\zeta-\hat{\zeta})(a\zeta-1)}\right]\right. \\ &\quad\left.+\sum_{n=1}^{+\infty}\left[nA_n\zeta^{n-1} + (\eta_1-1)n\overline{A}_n\zeta^{-n-1}\right]\right\} \quad (1<|\zeta|<R) \end{aligned} \tag{31}$$

- In the circular inclusion S_3

$$\sigma_{zy}+\mathrm{i}\sigma_{zx} = -\mu_3\eta_2(\varepsilon_{zy}^*+\mathrm{i}\varepsilon_{zx}^*) + \mu_3\eta_2\frac{(a\zeta-1)^2}{a^2-1}\left[\sum_{n=1}^{+\infty}(-n)\overline{B}_nR^{2n}\zeta^{-n-1}\right] \quad (|\zeta|>R) \tag{32}$$

It can be observed from (32) that when the system is only subject to remote uniform loading or uniform eigenstrain, the stress field inside the circular inclusion is no longer uniform due to the *nonuniform* thickness of the interphase layer. The average stresses inside the circular inclusion also give important information regarding the overall understanding and behavior of the composite material. The average stresses within the inner circular inclusion can be calculated to be

$$\bar{\sigma}_{zy}+\mathrm{i}\bar{\sigma}_{zx} = -\mu_3\eta_2(\varepsilon_{zy}^*+\mathrm{i}\varepsilon_{zx}^*) - \mu_3\eta_2\frac{(a^2R^2-1)^2}{R^2(a^2-1)}\sum_{n=1}^{+\infty}na^{-n-1}\overline{B}_n \tag{33}$$

where the bar "−" denotes the average value.

Following the approach of Gong and Meguid (1992), the change of elastic energy ΔW in the body due to the introduction of the coated circular inclusion can be evaluated for the case of uniform shearing σ_{zy}^{∞} and σ_{zx}^{∞} as

$$\Delta W = \frac{\pi}{\mu_1}\left[(\sigma_{zy}^{\infty})^2+(\sigma_{zx}^{\infty})^2\right]\left[(1-\eta_1)+\eta_1(1-\eta_2)(2-\eta_1)\sum_{n=1}^{+\infty}\frac{n(1-a^2)^2a^{-2(n+1)}}{(1-\eta_1)(1-\eta_2)-R^{2n}}\right] \tag{34}$$

When $\mu_2 = \mu_3$, i.e., $\eta_2 = 1$, then we have

$$\Delta W = \frac{\pi(1-\eta_1)}{\mu_1}\left[(\sigma_{zy}^{\infty})^2 + (\sigma_{zx}^{\infty})^2\right] \tag{35}$$

which coincides with the results of Gong and Meguid (1992).

Here we will term those coated inclusions, which satisfy $\Delta W = 0$, *stealth*. This definition for stealth inclusion can be considered as a natural extension for a uniformly coated inclusion (Honein et al., 1994). As a result, the nonuniformly coated inclusion will be stealth when

$$(1-\eta_1) + \eta_1(1-\eta_2)(2-\eta_1)\sum_{n=1}^{+\infty}\frac{n(1-a^2)^2 a^{-2(n+1)}}{(1-\eta_1)(1-\eta_2) - R^{2n}} = 0 \tag{36}$$

When the interphase thickness is uniform, i.e., $a \to +\infty$ and $R_0 = 1/R$, then

$$1 - \eta_1 = R_0^2(1-\eta_2) \tag{37}$$

The above condition is identical to that given by Honein et al. (1994).

4.3. Image force on the dislocation

Substituting the stress field acting on the screw dislocation (Eq. (30) subtracting the stress due to the dislocation itself) into the Peach–Koehler formula (Wang and Lee, 1999), we can obtain the image force on the screw dislocation. In the absence of external loading and uniform eigenstrain, i.e., $K = 0$, $\omega = 0$, the image force on the screw dislocation can be explicitly expressed as

$$F_x - \mathrm{i}F_y = \mu_1 2\pi q \frac{(a\hat{\zeta}-1)^2}{a^2-1}\left[(\eta_1 - 1)\frac{\bar{q}(1-a\overline{\hat{\zeta}})}{(|\hat{\zeta}|^2-1)(\hat{\zeta}-a)} + \eta_1\sum_{n=1}^{+\infty} nA_n\hat{\zeta}^{n-1}\right] \quad (|\hat{\zeta}| < 1) \tag{38}$$

5. A radial crack in the matrix

We now assume that a crack $[\hat{x}_1, \hat{x}_2]$ lies on the x-axis in the matrix as shown in Fig. 3, and we do not consider the uniform eigenstrains imposed on the circular inclusion. Applying the analytical solution for a screw dislocation which has been derived in the previous section, we finally obtain the following standard singular integral equations for the unknown dislocation densities $B(t)$

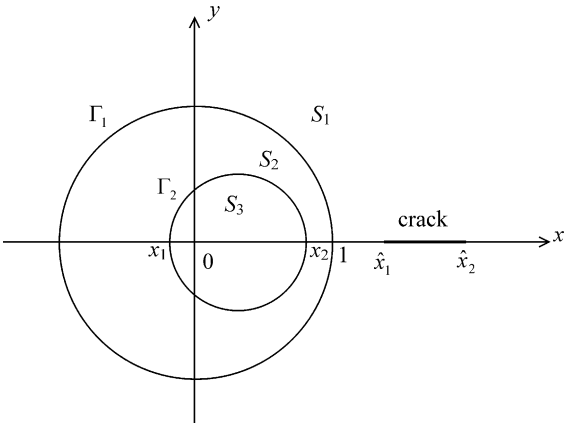

Fig. 3. A radial crack in the matrix interacting with the nonuniformly coated circular inclusion.

$$\int_{t_1}^{t_2} \frac{B(t)}{t-\xi}\,\mathrm{d}t + \int_{t_1}^{t_2} \left[\frac{1-\eta_1}{\xi - 1/t} - \eta_1(\eta_1-2)(\eta_2-1)\sum_{n=1}^{+\infty} \frac{t^n \xi^{n-1}}{(1-\eta_1)(1-\eta_2)-R^{2n}} \right] B(t)\,\mathrm{d}t$$
$$= \frac{2\pi\sigma_{zy}^{\infty}}{\mu_1} \frac{(a^2-1)}{a^2} \left[\frac{1}{(\xi - 1/a)^2} + \frac{a^2(1-\eta_1)}{(\xi-a)^2} + \eta_1(\eta_1-2)(\eta_2-1)\sum_{n=1}^{+\infty} \frac{n a^{1-n}\xi^{n-1}}{(1-\eta_1)(1-\eta_2)-R^{2n}} \right]$$
$$(t_1 < \xi < t_2) \tag{39}$$

and the uniqueness condition

$$\int_{t_1}^{t_2} B(t)\,\mathrm{d}t = 0 \tag{40}$$

where

$$t_1 = m(\hat{x}_1); \quad t_2 = m(\hat{x}_2) \tag{41}$$

It shall be noticed that the above singular integral equations are formulated in the ζ-plane in stead of in the original z-plane. Assuming square root singularities at both ends of the crack, the unknown dislocation density may be expressed as

$$B(t) = \frac{G(t)}{(t-t_1)^{0.5}(t_2-t)^{0.5}} \tag{42}$$

Following the simple numerical method developed by Erdogan and Gupta (1972), the discretized forms of Eqs. (39) and (40) can be obtained. Consequently, we can obtain the numerical solution of the dislocation density function $G(t)$ by solving the resulting linear algebraic equations. The stress component σ_{zy} behaves singularly at the two crack tips as follows

$$\sigma_{zy} = \frac{K(\hat{x}_1)}{\sqrt{2(\hat{x}_1 - x)}}; \quad \sigma_{zy} = \frac{K(\hat{x}_2)}{\sqrt{2(x-\hat{x}_2)}} \tag{43}$$

where

$$K(\hat{x}_1) = \frac{-\mu_1 G(t_1)|at_1 - 1|}{\sqrt{2(a^2-1)}} \frac{1}{\sqrt{t_2 - t_1}} \tag{44a}$$

$$K(\hat{x}_2) = \frac{\mu_1 G(t_2)|at_2 - 1|}{\sqrt{2(a^2-1)}} \frac{1}{\sqrt{t_2 - t_1}} \tag{44b}$$

The SIFs are defined as (Erdogan et al., 1991)

$$k_3(\hat{x}_1) = \lim_{x\to\hat{x}_1} \sqrt{2(\hat{x}_1 - x)}\,\sigma_{zy}(x,0) = K(\hat{x}_1)$$
$$k_3(\hat{x}_2) = \lim_{x\to\hat{x}_2} \sqrt{2(x - \hat{x}_2)}\,\sigma_{zy}(x,0) = K(\hat{x}_2) \tag{45}$$

6. Numerical examples and discussions

In all of the numerical results presented below, if unspecified, it is assumed that the radius of the circular inclusion S_3 is fixed to be 0.25, i.e., $R_0 = 0.25$.

6.1. The case of remote uniform shearing

In this subsection, we only consider the case in which the unbounded matrix is only subject to remote uniform shearing σ_{zy}^{∞}.

- Nonuniform stresses within the circular inclusion S_3

Figs. 4–7 illustrate the stress distribution in the circular inclusion along the circle Γ_2 and along the x-axis and y_1-axis (see Fig. 1) when the center of the circular inclusion S_3 is varied with $\mu_3{:}\mu_2{:}\mu_1 = 10{:}1{:}5$. It can be observed from Figs. 4–7 that the stress field inside the circular inclusion is still uniform when the thickness of the interphase layer is uniform, i.e., $x_2 = 0.25$. The uniform stress field calculated here is in agreement with that obtained by Honein et al. (1994). It can be clearly observed from these four figures that the nonuniformity of the stresses inside the circular inclusion is very strong when the interphase thickness is not uniform. When the inner circle is nearly in contact with the outer circle, the nonuniformity of the stresses in the inclusion is most apparent.

- Peak stresses

Fig. 8 presents the peak stresses $\sigma_{\text{peak}} = \max\left\{\sqrt{\sigma_{zx}^2 + \sigma_{zy}^2}\right\}$ at the interface Γ_2, which occur at $[x_2, 0]$, versus Δ and μ_2 with $\mu_3{:}\mu_1 = 2{:}1$. We observe that the magnitude of the peak stresses will also be lowered when the interphase layer becomes more compliant. The peak stresses are very sensitive to different values of Δ.

- Stress concentration

In the following, we consider the special case, where the circular inclusion S_3 is a hole. We are concerned with the stress concentration $\sigma_{zy}/\sigma_{zy}^{\infty}$ at the point of free edge $[x_2, 0]$. Fig. 9 shows the variation of the stress concentration versus Δ and μ_2/μ_1. It is noticed that when $\mu_1 = \mu_2$, the stress concentration is 2, which is the well known result for a cavity in an unbounded matrix. When $\mu_1 > \mu_2$ (the interphase layer is softer than the matrix), the stress concentration will be less than 2, in addition, when Γ_2 approaches Γ_1, the stress concentration will be lowered. When $\mu_1 < \mu_2$ (the interphase layer is stiffer than the matrix), the stress concentration will be larger than 2, and in addition, when Γ_2 is nearly in contact with Γ_1, the stress con-

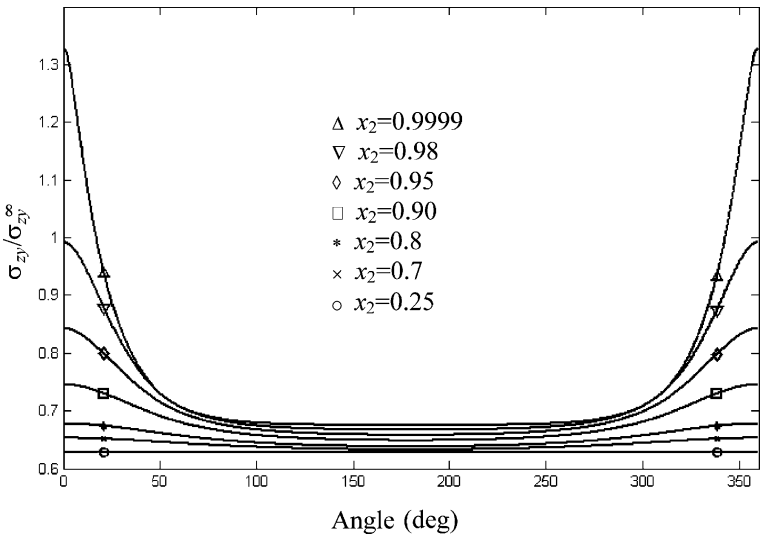

Fig. 4. Nonuniformity of normalized stress $\sigma_{zy}/\sigma_{zy}^{\infty}$ along the circular interface Γ_2.

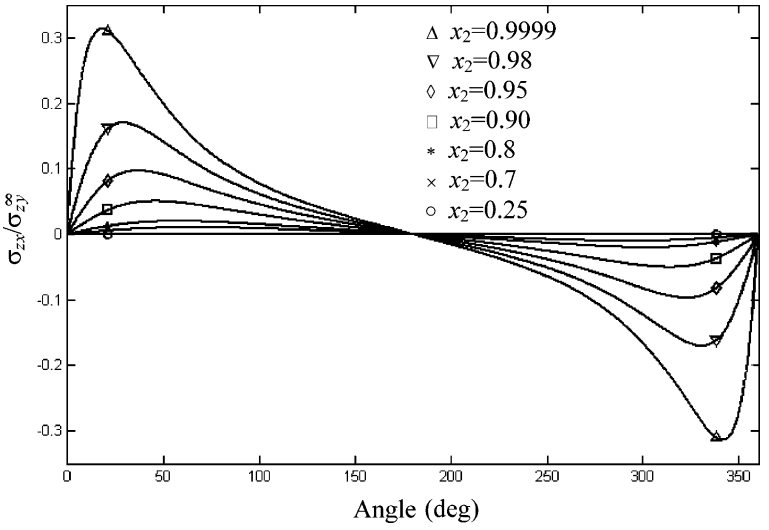

Fig. 5. Nonuniformity of normalized stress $\sigma_{zx}/\sigma_{zy}^{\infty}$ along the circular interface Γ_2.

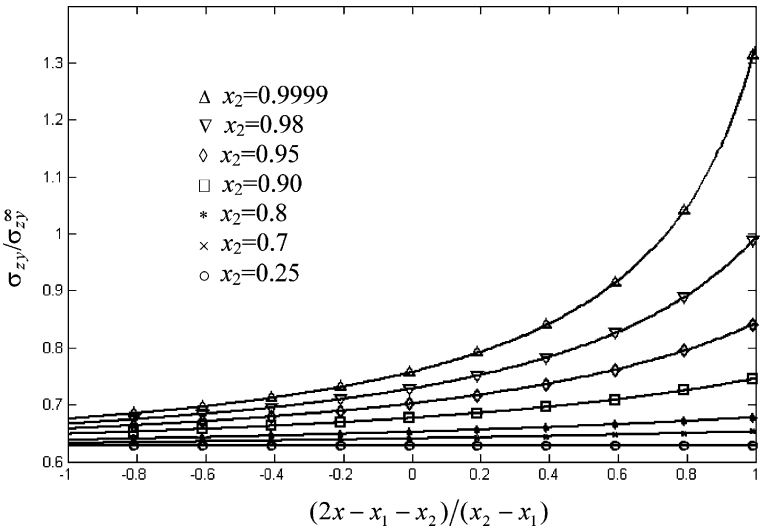

Fig. 6. Nonuniformity of normalized stress $\sigma_{zy}/\sigma_{zy}^{\infty}$ along the x-axis.

centration will be enhanced considerably, e.g., the stress concentration can get a value of 6 when $\Delta = 0.75$ and $\mu_2/\mu_1 = 3$.

6.2. Eigenstrain problem

It is assumed that the uniform eigenstrains imposed on the circular inclusion satisfy the following condition

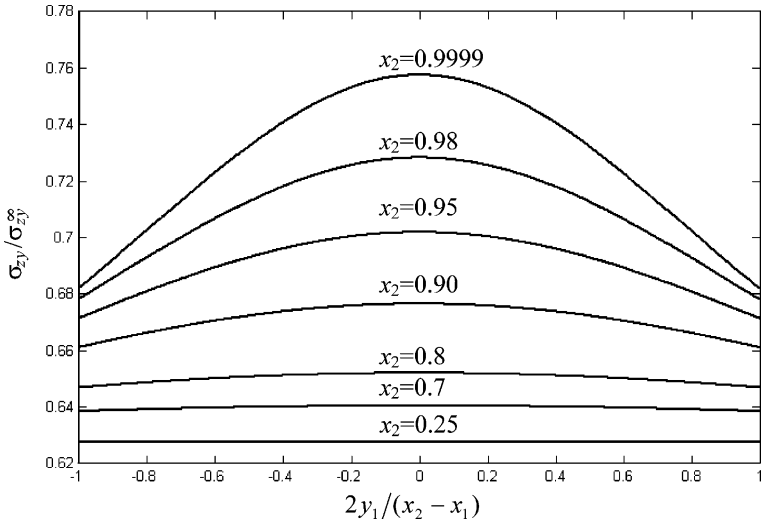

Fig. 7. Nonuniformity of normalized stress $\sigma_{zy}/\sigma_{zy}^{\infty}$ along the y_1-axis.

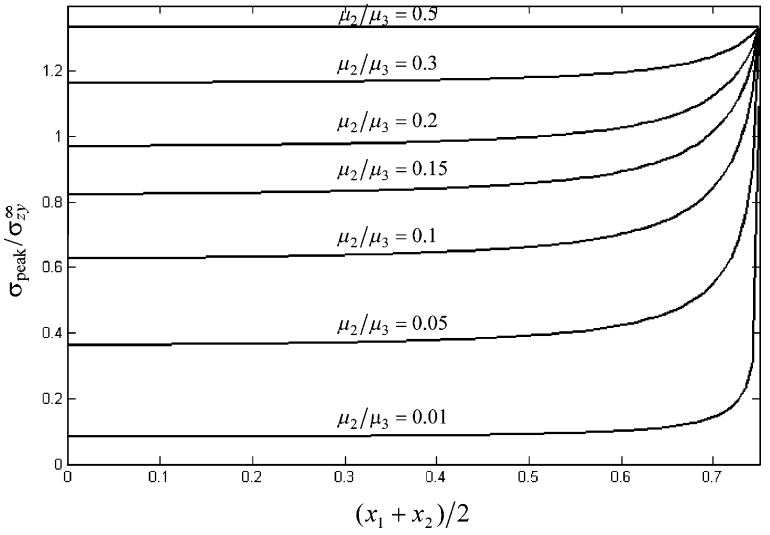

Fig. 8. Variations of peak stresses $\sigma_{peak}/\sigma_{zy}^{\infty}$ along the interface Γ_2 versus Δ and μ_2.

$$\varepsilon_{zx}^{*} = -\frac{1}{\mu_3}, \quad \varepsilon_{zy}^{*} = 0 \tag{46}$$

Fig. 10 shows the variations of stress component σ_{zx} along the x-axis when the stiffness of the interphase layer is varied with $x_2 = 0.9999$ and $\mu_1/\mu_3 = 0.5$. It can be observed that the nonuniformity of stress inside the circular inclusion is very strong when $\mu_2/\mu_3 \neq 0.5$ due to the varying interphase thickness. When $\mu_2/\mu_3 = 0.5$, the stress field inside the circular inclusion is still uniform since in this special case, the interphase layer and the matrix possess the same elastic properties. The magnitude of σ_{zx} will be lowered when the interphase layer becomes more compliant, while the magnitude of σ_{zx} at $x = 0.5$ will be elevated considerably when the interphase layer becomes stiffer than both the inclusion and the matrix.

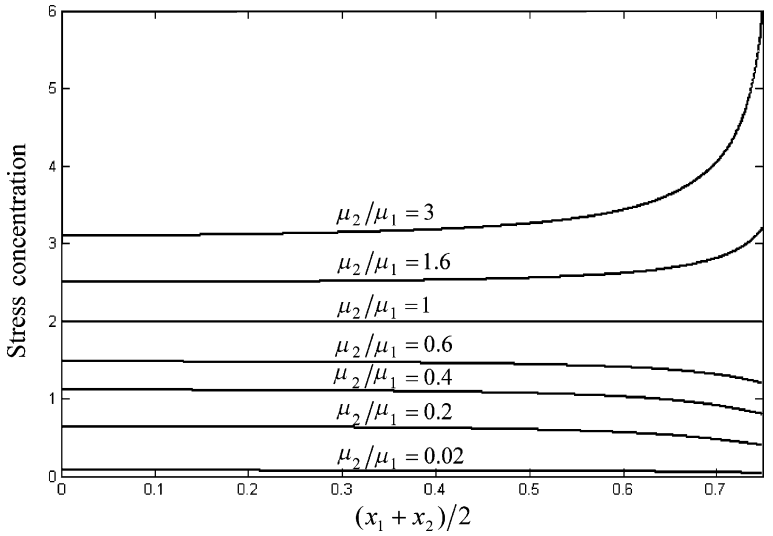

Fig. 9. Variation of the stress concentration versus Δ and μ_2/μ_1.

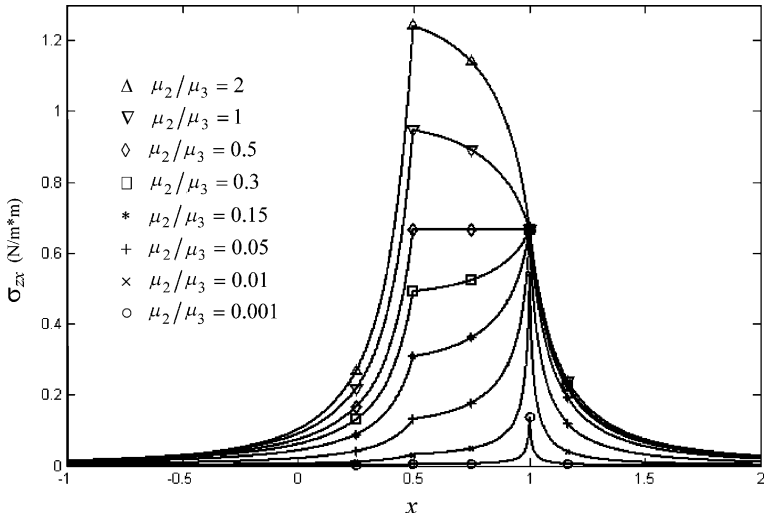

Fig. 10. Variations of σ_{zx} along the x-axis when the stiffness of the interphase layer is varied with $x_2 = 0.9999$ and $\mu_1/\mu_3 = 0.5$ when uniform eigenstrain is imposed on the circular inclusion.

6.3. Dislocation problem

In this subsection, we only consider the case of a screw dislocation with Burgers vector $\hat{b}$ on the x-axis in the unbounded matrix. In this case, $F_y = 0$ in view of (38). Fig. 11 shows the variation of $F^* = F_x/2\pi\mu_1\hat{b}^2$ versus the dislocation location and x_2 with $\mu_3{:}\mu_2{:}\mu_1 = 20{:}1{:}10$. This configuration represents that the inclusion is stiffer and the interphase layer is softer than the matrix. We find an interesting phenomenon that when the two circles Γ_1 and Γ_2 are nearly in contact with each other at the point [1,0], there is an *unstable* equilibrium position very near the circle Γ_1, and somewhat unexpectedly, there exists another *stable*

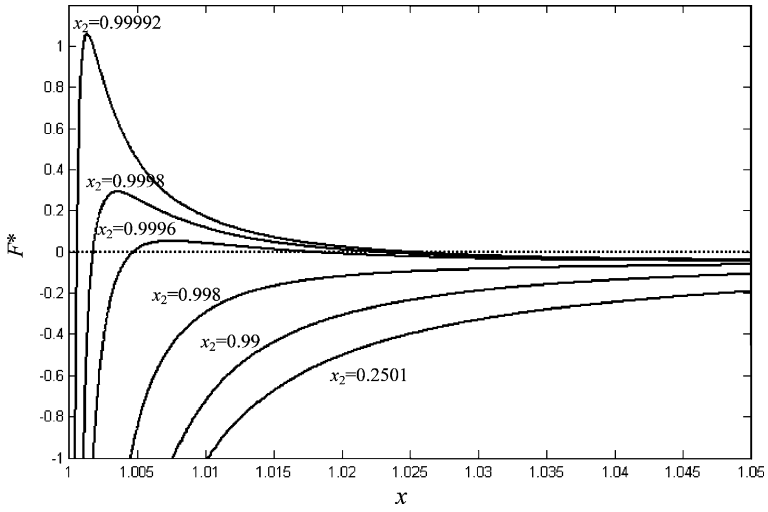

Fig. 11. Variation of $F^* = F_x/2\pi\mu_1\hat{b}_z^2$ versus the dislocation location and x_2 with μ_3:μ_2:$\mu_1 = 20$:1:10.

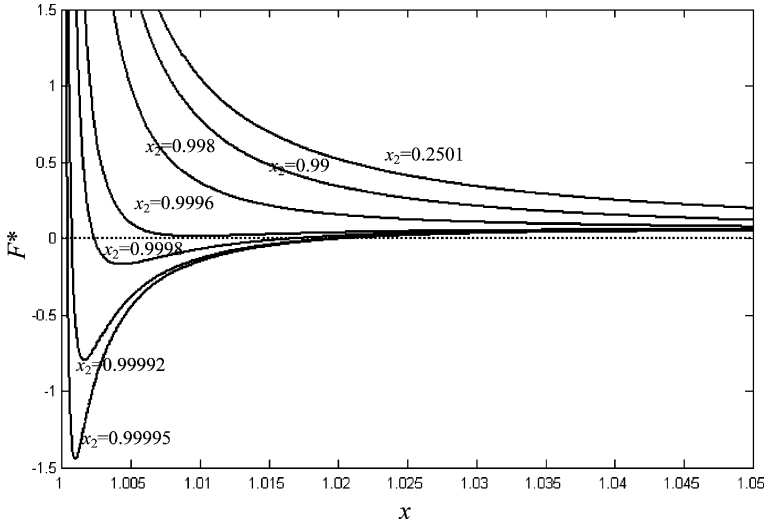

Fig. 12. Variation of $F^* = F_x/2\pi\mu_1\hat{b}_z^2$ versus the dislocation location and x_2 with μ_3:μ_2:$\mu_1 = 1$:24:2.

equilibrium position further away from the circle Γ_1. The numerical results of Xiao and Chen (2000) showed that the equilibrium positions are always unstable for a screw dislocation interacting with a *uniformly* coated fiber when the fiber is stiffer and the interphase layer is softer than the matrix. Fig. 12 shows the variation of $F^* = F_x/2\pi\mu_1\hat{b}^2$ versus the dislocation location and x_2 with μ_3:μ_2:$\mu_1 = 1$:24:2. This configuration represents that the inclusion is softer and the interphase layer is stiffer than the matrix. We can also find an interesting phenomenon that when the two circles Γ_1 and Γ_2 are nearly in contact with each other at the point [1,0], there is a *stable* equilibrium position very near the circle Γ_1, and somewhat unexpectedly, there exists another *unstable* equilibrium position further away from the circle Γ_1. The numerical results of Xiao and Chen (2000) showed that the equilibrium positions are always stable for a screw

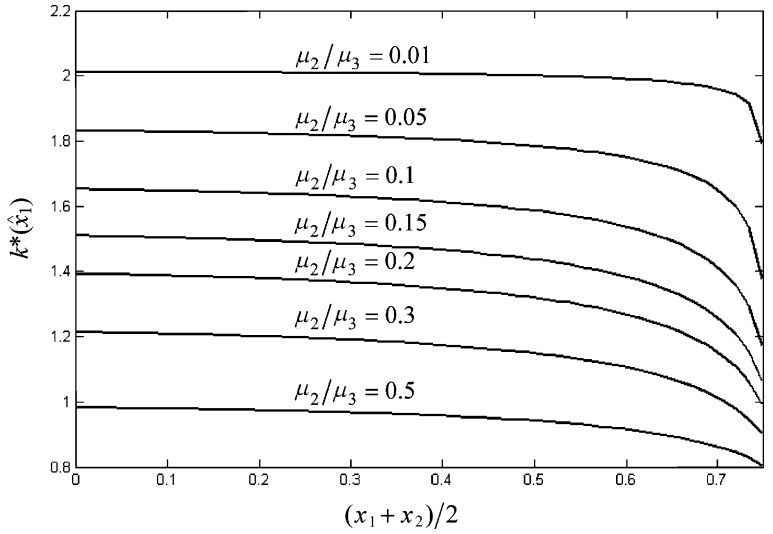

Fig. 13. Variations of the SIF $k^*(\hat{x}_1)$ versus Δ and μ_2 with μ_3:$\mu_1 = 2$:1 and $\hat{x}_1 = 1.05$, $\hat{x}_2 = 1.35$.

dislocation interacting with a *uniformly* coated fiber when the fiber is softer and the interphase layer is stiffer than the matrix.

6.4. A radial matrix crack

Fig. 13 illustrates the variations of the normalized SIF $k^*(\hat{x}_1) = k_3(\hat{x}_1)/\sigma_{zy}^{\infty}\sqrt{0.5(\hat{x}_2 - \hat{x}_1)}$ versus Δ and μ_2 with μ_3:$\mu_1 = 2$:1 and $\hat{x}_1 = 1.05$, $\hat{x}_2 = 1.35$. It can be observed that the magnitude of SIF at $\hat{x}_1$ will be lowered when the nonuniformity of the compliant interphase layer increases, and that the magnitude of SIF will be elevated when the interphase layer is more compliant. Fig. 14 shows the difference in SIF

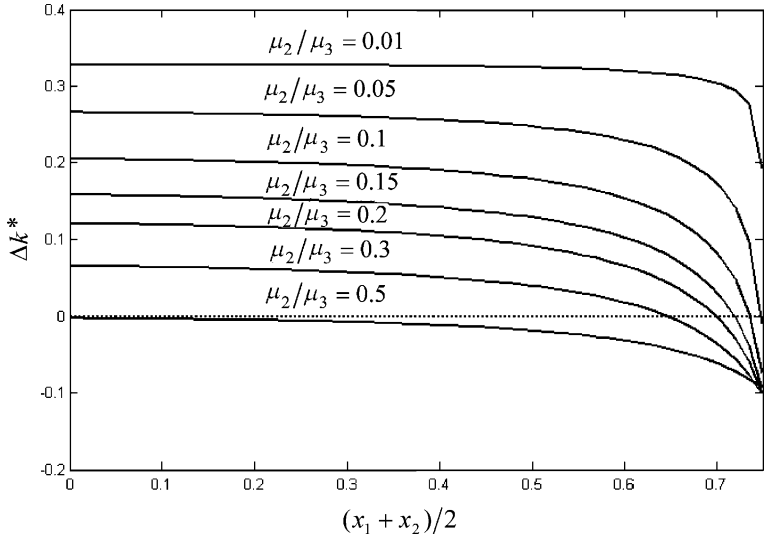

Fig. 14. Difference in SIF Δk^* versus Δ and μ_2 with μ_3:$\mu_1 = 2$:1 and $\hat{x}_1 = 1.05$, $\hat{x}_2 = 1.35$.

$\Delta k^* = (k_3(\hat{x}_1) - k_3(\hat{x}_2))/\sigma_{zy}^{\infty}\sqrt{0.5(\hat{x}_2 - \hat{x}_1)}$ versus Δ and μ_2 with $\mu_3{:}\mu_1 = 2{:}1$ and $\hat{x}_1 = 1.05$, $\hat{x}_2 = 1.35$. We can find that the difference in SIF can be positive or negative depending on the combinations of Δ and μ_2. It can also be noticed that Δk^* can just be equal to zero for some special combinations of Δ and μ_2.

7. Conclusions

The following conclusions, which are unique for the *nonuniformly* coated circular inclusion, can be drawn from this research

- When the three-phase composite system is only subject to remote uniform shearing or uniform eigenstrain imposed on the circular inclusion, the stress field inside the circular inclusion is intrinsically *nonuniform* due to the varying interphase thickness. It is not the average stresses but the peak stresses that can describe where the debonding and failure will occur.
- When a screw dislocation interacts with the nonuniformly coated circular inclusion, two equilibrium positions of *different nature*, one stable and the other one unstable, may coexist.

The analytical solution for a screw dislocation is also applied as Green's function to study matrix cracking in the inclusion/interphase/matrix composite system. It is observed that the varying interphase thickness can significantly affect SIF.

Acknowledgements

The authors are greatly indebted to a referee for his/her very helpful comments and suggestions. This work was supported by the National Excellent Young Scholar Science Fund of China (Project no. 10125209), the National Natural Science Foundation of China (Project no. 10072041) and the Teaching and Research Award Fund for Outstanding Young Teachers in High Education Institutions of MOE, PR China.

References

Achenbach, J.D., Zhu, H., 1990. Effect of interphases on micro and macromechanical behavior of hexagonal-array fiber composites. ASME J. Appl. Mech. 57, 956–963.

Cao, W.J., 1988. Conformal Mapping Theory and its Application. Shanghai Science and Technology Press, Shanghai, China (in Chinese).

Gong, S.X., Meguid, S.A., 1992. A general treatment of the elastic field of an elliptical inhomogeneity under antiplane shear. ASME J. Appl. Mech. 59, 131–135.

Erdogan, F., Gupta, G.D., 1972. On the numerical solution of singular integral equations. Quart. Appl. Math. 30, 525–534.

Erdogan, F., Kaya, A.C., Joseph, P.F., 1991. The mode-III crack problem in bonded materials with a nonhomogeneous interfacial zone. ASME J. Appl. Mech. 58, 419–427.

Honein, T., Honein, E., Herrmann, G., 1994. Circularly cylindrical and plane layered media in antiplane elastostatics. ASME J. Appl. Mech. 61, 243–249.

Liu, Y.J., Xu, N., Luo, J.F., 2000. Modeling of interphases in fiber-reinforced composites under transverse loading using the boundary element method. ASME J. Appl. Mech. 67, 41–49.

Liu, Y., Ru, C.Q., Schiavone, P., Mioduchowski, A., 2001. New phenomena concerning the effect of imperfect bonding on radial matrix crack in fiber composites. Int. J. Eng. Sci. 39, 2033–2050.

Muskhelishvili, N.I., 1953. Some Basic Problems of the Mathematical Theory of Elasticity. Noordhoff, Groningen.

Ru, C.Q., Schiavone, P., 1997. A circular inclusion with circumferentially inhomogeneous interface in antiplane shear. Proc. R. Soc. Lond. 453, 2551–2572.

Ru, C.Q., Schiavone, P., Mioduchowski, A., 1999. Uniformity of stresses within a three-phase elliptic inclusion in anti-plane shear. J. Elasticity 52, 121–128.

Shen, H., Schiavone, P., Ru, C.Q., Mioduchowski, A., 2000. An elliptic inclusion with imperfect interface in anti-plane shear. Int. J. Solids Struct. 37, 4557–4575.

Shen, H., Schiavone, P., Ru, C.Q., Mioduchowski, A., 2001a. Stress analysis of an elliptic inclusion with imperfect interface in plane elasticity. J. Elasticity 62, 25–46.

Shen, H., Schiavone, P., Ru, C.Q., Mioduchowski, A., 2001b. Interfacial thermal stress analysis of an elliptic inclusion with a compliant interphase layer in plane elasticity. Int. J. Solids Struct. 38, 7587–7606.

Shodja, H.M., Sarvestani, A.S., 2001. Elastic fields in double inhomogeneity by the equivalent inclusion method. ASME J. Appl. Mech. 68, 3–10.

Wang, S.D., Lee, S., 1999. Screw dislocation near a slant edge crack. Mech. Mater. 31, 63–70.

Xiao, Z.M., Chen, B.J., 2000. A screw dislocation interacting with a coated fiber. Mech. Mater. 32, 485–494.

Xiao, Z.M., Chen, B.J., 2001a. An edge dislocation interacting with a coated fiber. Int. J. Solids Struct. 38, 2533–2548.

Xiao, Z.M., Chen, B.J., 2001b. Stress analysis for a Zener–Stroh crack interacting with a coated inclusion. Int. J. Solids Struct. 38, 5007–5018.

Zhong, Z., Meguid, S.A., 1997. On the elastic field of a spherical inhomogeneity with an imperfectly bonded interface. J. Elasticity 46, 91–113.